Supporting information for: How do brassinosteroids activate their receptors?

Alexander S. Moffett[1] and Diwakar Shukla[1,2,3,4]

[1]Center for Biophysics and Quantitative Biology, University of Illinois at Urbana-Champaign
[2]Department of Chemical and Biomolecular Engineering, University of Illinois at Urbana-Champaign
[3]Department of Plant Biology, University of Illinois at Urbana-Champaign
[4]Beckman Institute for Advanced Science and Technology, University of Illinois at Urbana-Champaign

BRI1 E749 protonation

For the sake of completeness, we report results for BRI1 E749, although BRI1 E749 is unlikely to be protonated at pH 5 (Fig. S25). Counterintuitively, protonation of tBRI1 E749 appeared to strongly stabilize both the apo and holo tBRI1-BAK1 complex (Fig. S24 C-D). As BRI1 E749 interacts with BAK1 R146 in crystal structures (Fig. 1), we expected protonation of BRI1 E749 to break this interaction and weaken the stability of the rBRI1-BAK1 complex. However, for protonation of tBRI1 E749 we estimated $\Delta\Delta G_{Apo} = -12.225 \pm 0.101$ kcal·mol^{-1} and $\Delta\Delta G_{Holo} = -7.113 \pm 0.102$ kcal·mol^{-1}. It appears that the interaction partners of BRI1 E749 in BAK1 are involved in unrealistic interactions with the truncated C-terminus of tBRI1.

Calculation of association free energies from previously reported dissociation constants

Here, we show our calculations for binding free energy given the dissociation constants obtained by Hohmann and coworkers [1]. We assume a temperature of 300 K and use a standard concentration of $C^\circ = 1/(1661\ \text{Å}^3)$. The standard free energy of association between the BAK1 and BL-bound BRI1 extracellular domains was calculated from grating-coupled interferometry results as follows:

$$K_D = 0.71\ \mu M = 0.71 \frac{\mu\text{mol}}{L} \cdot \frac{1\ \text{mol}}{10^6\ \mu\text{mol}} \cdot \frac{1\ L}{10^{27}\ \text{Å}^3} \cdot 6.022 \cdot 10^{23}\ \text{mol}^{-1} \approx 4.28 \cdot 10^{-10}\text{Å}^{-3}$$

$$K_A = \frac{1}{K_D} \approx 2.34 \cdot 10^9\ \text{Å}^3$$

$$\Delta G^\circ = -RT \log(K_A/1661\ \text{Å}^3) \approx -8.44\ \text{kcal} \cdot \text{mol}^{-1}$$

The free energy of association from isothermal titration calorimetry (-9.20 kcal·mol^{-1}) was calculated accordingly.

Calculation of association free energies from REUS

For the sake of brevity, we use the following shorthand notation for averages: $\langle A(\mathbf{x})\rangle^E_{\{\alpha,\beta,\gamma,\dots\}}$, where $A(\mathbf{x})$ is the quantity, dependent on protein coordinates, to be averaged, the superscript E denotes the state of the

association progress, either at the binding site (S) or in bulk solution (B), and $\{\alpha, \beta, \gamma \dots\}$ represents the set of collective variables restrained when the average is taken. For example,

$$\langle e^{-\beta u_\Theta(\mathbf{x})} \rangle^S_{\{BR,BA\}} = \frac{\int_S e^{-\beta[U(\mathbf{x})+pV(\mathbf{x})+u_{BR}(\mathbf{x})+u_{BA}(\mathbf{x})+u_\Theta(\mathbf{x})]} d\mathbf{x}}{\int_S e^{-\beta[U(\mathbf{x})+pV(\mathbf{x})+u_{BR}(\mathbf{x})+u_{BA}(\mathbf{x})]} d\mathbf{x}} \tag{1}$$

is the average value of $e^{-\beta u_\Theta(\mathbf{x})}$ in the NPT ensemble, $u_\Theta(\mathbf{x})$ being the restraint potential on Θ, with BRI1 and BAK1 bound and with the BRI1 and BAK1 backbone atoms restrained. The overall calculations of standard association free energies proceed as follows:

$$\Delta G^S_{BR} = \beta^{-1} \ln \left[\langle e^{-\beta u_{BR}(\mathbf{x})} \rangle^S \right] \tag{2}$$
$$\Delta G^S_{BA} = \beta^{-1} \ln \left[\langle e^{-\beta u_{BA}(\mathbf{x})} \rangle^S_{\{BR\}} \right] \tag{3}$$
$$\Delta G^S_{\Theta} = \beta^{-1} \ln \left[\langle e^{-\beta u_{\Theta}(\mathbf{x})} \rangle^S_{\{BR,BA\}} \right] \tag{4}$$
$$\Delta G^S_{\Phi} = \beta^{-1} \ln \left[\langle e^{-\beta u_{\Phi}(\mathbf{x})} \rangle^S_{\{BR,BA,\Theta\}} \right] \tag{5}$$
$$\Delta G^S_{\Psi} = \beta^{-1} \ln \left[\langle e^{-\beta u_{\Psi}(\mathbf{x})} \rangle^S_{\{BR,BA,\Theta,\Phi\}} \right] \tag{6}$$
$$\Delta G^S_{\phi} = \beta^{-1} \ln \left[\langle e^{-\beta u_{\phi}(\mathbf{x})} \rangle^S_{\{BR,BA,\Theta,\Phi,\Psi\}} \right] \tag{7}$$
$$\Delta G^S_{\theta} = \beta^{-1} \ln \left[\langle e^{-\beta u_{\theta}(\mathbf{x})} \rangle^S_{\{BR,BA,\Theta,\Phi,\Psi,\phi\}} \right] \tag{8}$$
$$\Delta G^S_{BL} = \beta^{-1} \ln \left[\langle e^{-\beta u_{BL}(\mathbf{x})} \rangle^S_{\{BR,BA,\Theta,\Phi,\Psi,\phi,\theta\}} \right] \tag{9}$$
$$\Delta G^B_{BL} = \beta^{-1} \ln \left[\langle e^{-\beta u_{BL}(\mathbf{x})} \rangle^B_{\{BR,BA,\Theta,\Phi,\Psi,\phi,\theta\}} \right] \tag{10}$$
$$\Delta G^B_{\theta} = \beta^{-1} \ln \left[\langle e^{-\beta u_{\theta}(\mathbf{x})} \rangle^B_{\{BR,BA,\Theta,\Phi,\Psi,\phi\}} \right] \tag{11}$$
$$\Delta G^B_{\phi} = \beta^{-1} \ln \left[\langle e^{-\beta u_{\phi}(\mathbf{x})} \rangle^B_{\{BR,BA,\Theta,\Phi,\Psi\}} \right] \tag{12}$$
$$\Delta G^B_{\Psi} = \beta^{-1} \ln \left[\langle e^{-\beta u_{\Psi}(\mathbf{x})} \rangle^B_{\{BR,BA,\Theta,\Phi\}} \right] \tag{13}$$
$$\Delta G^B_{\Phi} = \beta^{-1} \ln \left[\langle e^{-\beta u_{\Phi}(\mathbf{x})} \rangle^B_{\{BR,BA,\Theta\}} \right] \tag{14}$$
$$\Delta G^B_{\Theta} = \beta^{-1} \ln \left[\langle e^{-\beta u_{\Theta}(\mathbf{x})} \rangle^B_{\{BR,BA\}} \right] \tag{15}$$
$$\Delta G^B_{BA} = \beta^{-1} \ln \left[\langle e^{-\beta u_{BA}(\mathbf{x})} \rangle^B_{\{BR\}} \right] \tag{16}$$
$$\Delta G^B_{BR} = \beta^{-1} \ln \left[\langle e^{-\beta u_{BR}(\mathbf{x})} \rangle^B \right] \tag{17}$$
$$\Delta G^S_0 = \Delta G^S_{\Theta} + \Delta G^S_{\Phi} + \Delta G^S_{\Psi} + \Delta G^S_{\theta} + \Delta G^S_{\phi} \tag{18}$$
$$\Delta G^B_0 = \Delta G^B_{\Theta} + \Delta G^B_{\Phi} + \Delta G^B_{\Psi} = -\beta^{-1} \ln \left[\frac{1}{8\pi^2} \int_0^\pi \int_0^{2\pi} \int_0^{2\pi} \sin(\Theta) e^{-\beta u_0(\Theta,\Phi,\Psi)} d\Psi d\Phi d\Theta \right] \tag{19}$$
$$I^* = \int_{bound} e^{-\beta[W(r)-W(r^*)]} dr \tag{20}$$
$$O^* = (r^*)^2 \int_0^\pi \int_0^{2\pi} \sin(\theta) e^{-\beta u_a(\theta,\phi)} d\theta d\phi \tag{21}$$
$$K_A^{Apo} = O^* I^* e^{-\beta[(\Delta G^B_{BR} - \Delta G^S_{BR}) + (\Delta G^B_{BA} - \Delta G^S_{BA}) + (\Delta G^B_0 - \Delta G^S_0)]} \tag{22}$$
$$K_A^{BL} = O^* I^* e^{-\beta[(\Delta G^B_{BR} - \Delta G^S_{BR}) + (\Delta G^B_{BA} - \Delta G^S_{BA}) + (\Delta G^B_0 - \Delta G^S_0) + (\Delta G^B_{BL} - \Delta G^S_{BL})]} \tag{23}$$
$$\Delta G^\circ = -\beta^{-1} \ln \left[K_A C^\circ \right], \; C^\circ = \frac{1}{1661 \text{Å}^3} \tag{24}$$

Note that the O^* and ΔG^B_0 terms can be calculated analytically, as shown below, while each other term requires MD simulation.

Apo orientational restraint contribution

$$
\begin{aligned}
O^*_{Apo} &= (r^*)^2 \int_0^{\pi} \int_0^{2\pi} \sin(\Theta) e^{-\beta u_a(\Theta,\Phi)} d\Phi d\Theta \\
&= (44\ \text{Å})^2 \int_0^{2\pi} e^{-\beta(.5)(.1)(180/\pi)^2(\Phi - 16.8963(\pi/180))^2} d\Phi \int_0^{\pi} \sin(\Theta) e^{-\beta(.5)(.1)(180/\pi)^2(\Theta - 120.4496(\pi/180))^2} d\Theta \\
&= (1936\ \text{Å}^2)(0.106819)(0.0920026) = 19.0262\ \text{Å}^2
\end{aligned}
$$

Apo bulk angular restraint contributions

$$
\begin{aligned}
\Delta G^B_{0,Apo} &= -\beta^{-1} \ln \left[\frac{1}{8\pi^2} \int_0^{\pi} \int_0^{2\pi} \int_0^{2\pi} \sin(\Theta) e^{-\beta u_0(\Theta,\Phi,\Psi)} d\Psi d\Phi d\Theta \right] \\
&= -\beta^{-1} \ln \left[\frac{1}{8\pi^2} \int_0^{2\pi} e^{-\beta(.5)(.1)(180/\pi)^2(\Psi - 33.0273(\pi/180))^2} d\Psi \int_0^{2\pi} e^{-\beta(.5)(.1)(180/\pi)^2(\phi - 261.461(\pi/180))^2} d\phi \right. \\
&\left. \int_0^{\pi} \sin(\theta) e^{-\beta(.5)(.1)(180/\pi)^2(\theta - 73.4478(\pi/180))^2} d\theta \right] \\
&= 6.63\ \text{kcal} \cdot \text{mol}^{-1}
\end{aligned}
$$

Holo orientational restraint contribution

$$
\begin{aligned}
O^*_{Holo} &= (r^*)^2 \int_0^{\pi} \int_0^{2\pi} \sin(\Theta) e^{-\beta u_a(\Theta,\Phi)} d\Phi d\Theta \\
&= (44\ \text{Å})^2 \int_0^{2\pi} e^{-\beta(.5)(.1)(180/\pi)^2(\Phi - 15.9178(\pi/180))^2} d\Phi \int_0^{\pi} \sin(\Theta) e^{-\beta(.5)(.1)(180/\pi)^2(\Theta - 118.5843(\pi/180))^2} d\Theta \\
&= (1936\ \text{Å}^2)(0.106819)(0.0937143) = 19.3802\ \text{Å}^2
\end{aligned}
$$

Holo bulk angular restraint contributions

$$
\begin{aligned}
\Delta G^B_{0,Holo} &= -\beta^{-1} \ln \left[\frac{1}{8\pi^2} \int_0^{\pi} \int_0^{2\pi} \int_0^{2\pi} \sin(\Theta) e^{-\beta u_0(\Theta,\Phi,\Psi)} d\Psi d\Phi d\Theta \right] \\
&= -\beta^{-1} \ln \left[\frac{1}{8\pi^2} \int_0^{2\pi} e^{-\beta(.5)(.1)(180/\pi)^2(\Psi - 33.7587(\pi/180))^2} d\Psi \int_0^{2\pi} e^{-\beta(.5)(.1)(180/\pi)^2(\phi - 267.2762(\pi/180))^2} d\phi \right. \\
&\left. \int_0^{\pi} \sin(\theta) e^{-\beta(.5)(.1)(180/\pi)^2(\theta - 75.9999(\pi/180))^2} d\theta \right] \\
&= 6.62\ \text{kcal} \cdot \text{mol}^{-1}
\end{aligned}
$$

References

[1] Hohmann U, Santiago J, Nicolet J, Olsson V, Spiga FM, Hothorn LA, Butenko MA, Hothorn M. Mechanistic basis for the activation of plant membrane receptor kinases by SERK-family coreceptors. Proc Natl Acad Sci USA. 2018; p. 201714972. doi:10.1073/pnas.1714972115.

[2] Hunter JD. Matplotlib: A 2D graphics environment. Comput Sci Eng. 2007;9(3):90–95. doi:10.1109/MCSE.2007.55.

[3] Chodera JD. A simple method for automated equilibration detection in molecular simulations. J Chem Theory Comput. 2016;12(4):1799–1805. doi:10.1021/acs.jctc.5b00784.

[4] pymbar 3.0.4; https://pymbar.readthedocs.io/en/master/.

[5] Shirts MR, Chodera JD. Statistically optimal analysis of samples from multiple equilibrium states. J Chem Phys. 2008;129(12):124105. doi:10.1063/1.2978177.

[6] Søndergaard CR, Olsson MH, Rostkowski M, Jensen JH. Improved treatment of ligands and coupling effects in empirical calculation and rationalization of pK_a values. J Chem Theory Comput. 2011;7(7):2284–2295. doi:10.1021/ct200133y.

[7] Olsson MH, Søndergaard CR, Rostkowski M, Jensen JH. PROPKA3: consistent treatment of internal and surface residues in empirical pK_a predictions. J Chem Theory Comput. 2011;7(2):525–537. doi:10.1021/ct100578z.

Table S1: Force constants and reference collective variable values used for restraints in REUS PMF calculations.

Collective variable	k_{Force}	Apo reference	Holo reference
BRI1 RMSD	10.0*	1.1825 Å	1.1492 Å
BAK1 RMSD	10.0*	1.1973 Å	1.3730 Å
Θ	0.10†	120.4496°	118.5843°
Φ	0.10†	16.8963°	15.9178°
Ψ	0.10†	33.0273°	33.7587°
ϕ	0.10†	261.461°	267.2762°
θ	0.10†	73.4478°	75.9999°
BL-BRI1 distance	10.0*	N/A	18.7735 Å

*kcal·mol^{-1}·Å^{-2} †kcal·mol^{-1}·degree^{-2}

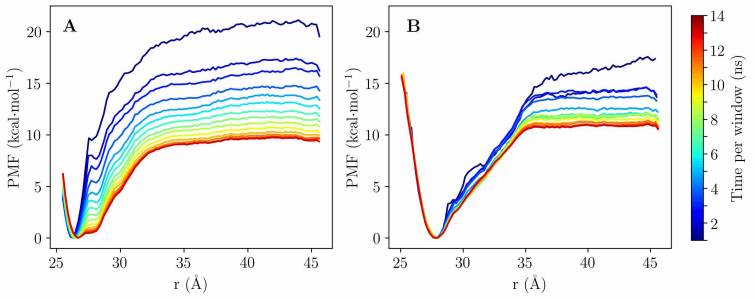

Figure S1: Convergence of the **A** apo and **B** holo tBRI1-BAK1 separation PMFs with REUS sampling time per window. This figure was produced using Matplotlib 2.2.2 [2].

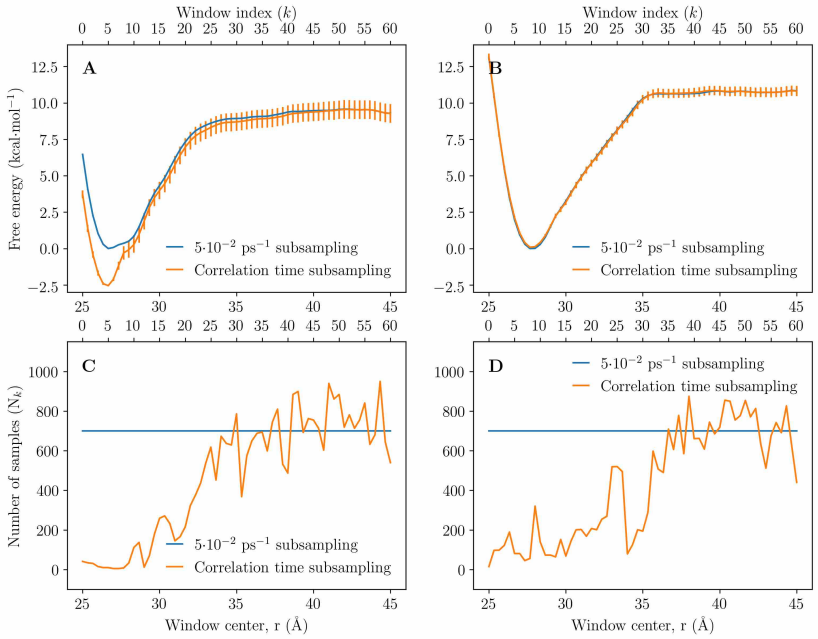

Figure S2: Rationale for our choice of a uniform 50 ns^{-1} subsampling rate for REUS simulations. **A** The apo and **B** holo separation PMFs using a uniform 50 ns^{-1} subsampling rate and a subsampling rate determined individually for each window using the correlation time method implemented in pymbar [3, 4]. The number of samples remaining for each window for the **C** apo and **D** holo systems. Using the correlation time to subsample yields uncorrelated samples but at the same time causes highly uneven sampling across r. Using a uniform subsampling time of 50 ns^{-1} by definition yields even sampling over r, but likely results in the use of correlated samples in some windows, leading to underestimation of error [5]. This figure was produced using Matplotlib 2.2.2 [2].

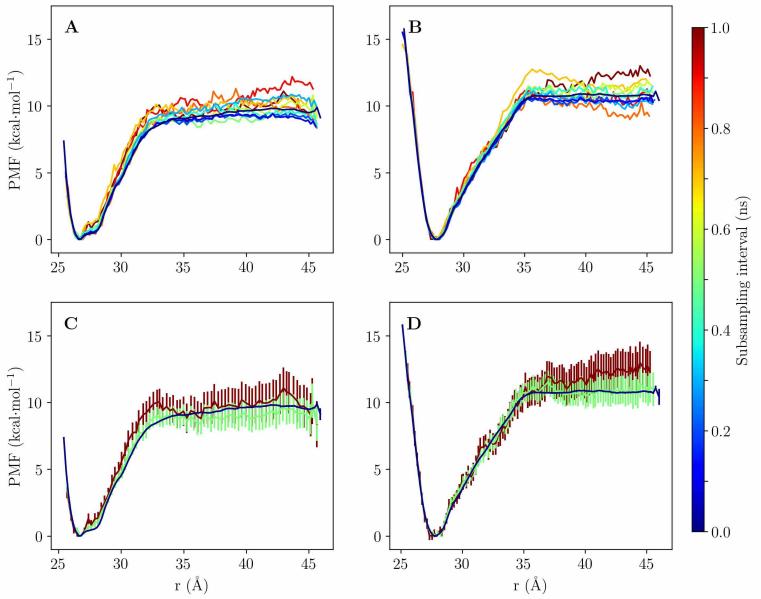

Figure S3: The effects of subsampling rate on the **A** apo and **B** holo separation PMFs. We chose three subsampling rates to include with error bars shown for the **C** apo and **D** holo separation PMFs. Note the general insensitivity to both separation PMFs to the choice of uniform subsampling rate over all windows. This figure was produced using Matplotlib 2.2.2 [2].

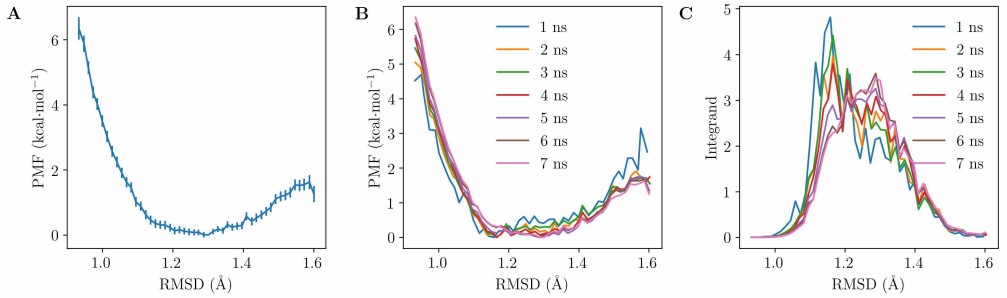

Figure S4: tBRI1 conformational restraint contributions for bound apo BRI1-BAK1. **A** The restraint PMF. **B** Convergence of the restraint PMF with simulation time. **C** Convergence of the integrand within the associated ensemble average estimation with time. This figure was produced using Matplotlib 2.2.2 [2].

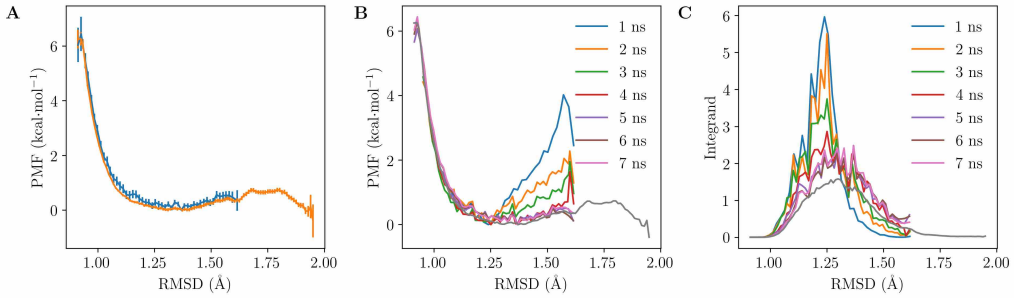

Figure S5: BAK1 conformational restraint contributions for bound apo BRI1-BAK1. **A** The restraint PMF. The PMF including additional umbrella sampling is shown in orange. **B** Convergence of the restraint PMF with simulation time. The PMF including additional umbrella sampling is shown in grey. **C** Convergence of the integrand within the associated ensemble average estimation with time. The integrand including additional umbrella sampling is shown in orange. This figure was produced using Matplotlib 2.2.2 [2].

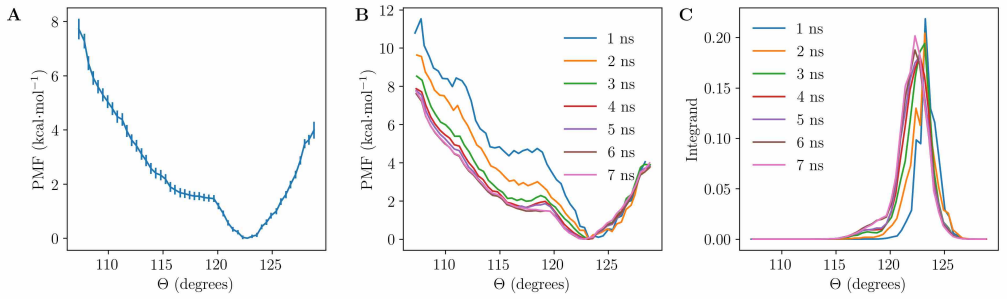

Figure S6: Θ restraint contributions for bound apo BRI1-BAK1. **A** The restraint PMF. **B** Convergence of the restraint PMF with simulation time. **C** Convergence of the integrand within the associated ensemble average estimation with time. This figure was produced using Matplotlib 2.2.2 [2].

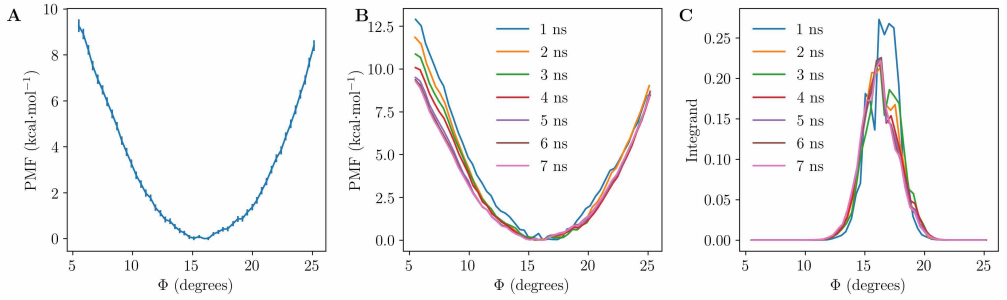

Figure S7: Φ restraint contributions for bound apo BRI1-BAK1. **A** The restraint PMF. **B** Convergence of the restraint PMF with simulation time. **C** Convergence of the integrand within the associated ensemble average estimation with time. This figure was produced using Matplotlib 2.2.2 [2].

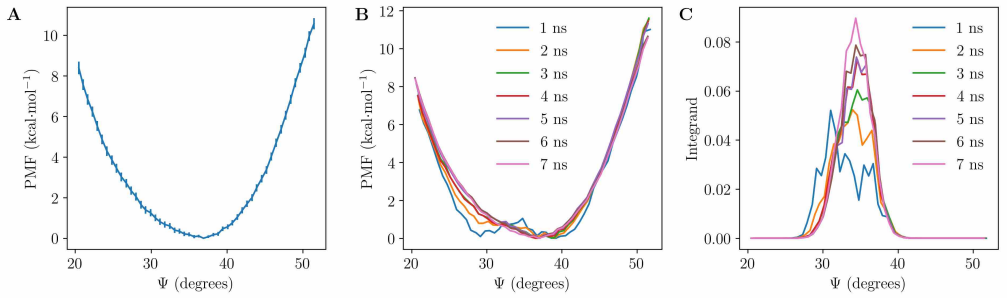

Figure S8: Ψ restraint contributions for bound apo BRI1-BAK1. **A** The restraint PMF. **B** Convergence of the restraint PMF with simulation time. **C** Convergence of the integrand within the associated ensemble average estimation with time. This figure was produced using Matplotlib 2.2.2 [2].

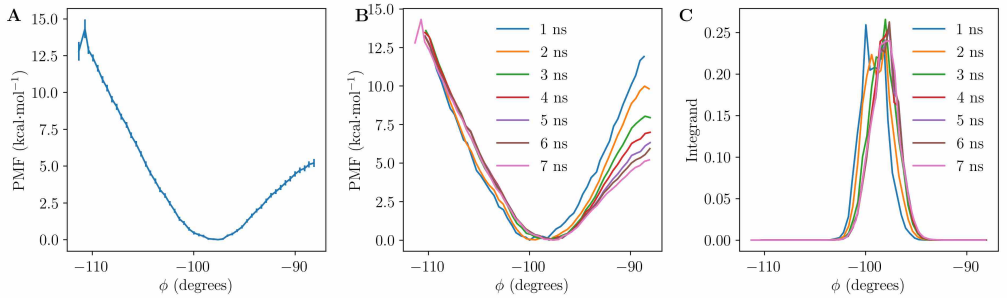

Figure S9: ϕ restraint contributions for bound apo BRI1-BAK1. **A** The restraint PMF. **B** Convergence of the restraint PMF with simulation time. **C** Convergence of the integrand within the associated ensemble average estimation with time. This figure was produced using Matplotlib 2.2.2 [2].

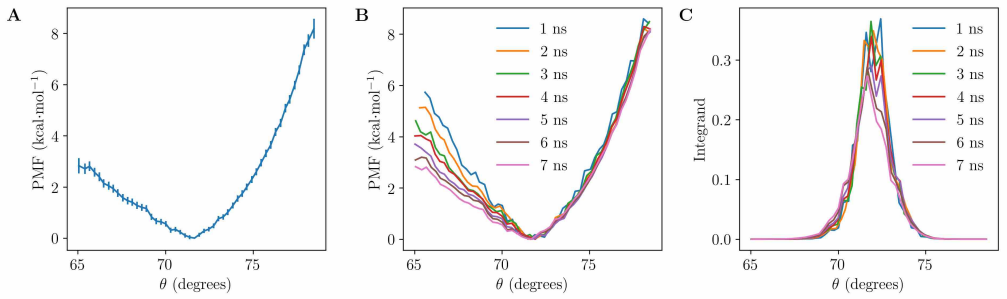

Figure S10: θ restraint contributions for bound apo BRI1-BAK1. **A** The restraint PMF. **B** Convergence of the restraint PMF with simulation time. **C** Convergence of the integrand within the associated ensemble average estimation with time. This figure was produced using Matplotlib 2.2.2 [2].

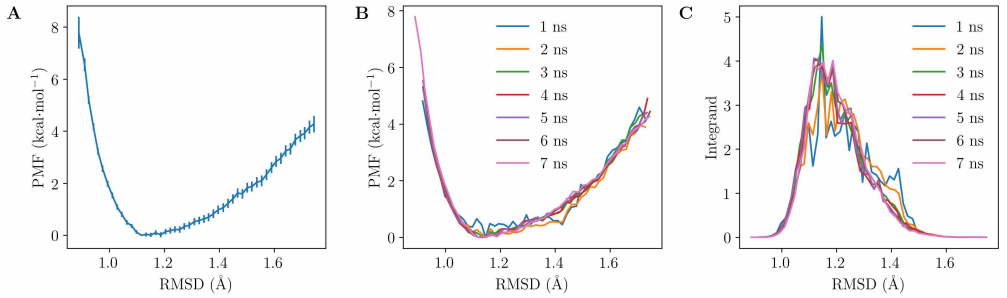

Figure S11: BAK1 conformational restraint contributions for unbound apo BRI1-BAK1. **A** The restraint PMF. **B** Convergence of the restraint PMF with simulation time. **C** Convergence of the integrand within the associated ensemble average estimation with time. This figure was produced using Matplotlib 2.2.2 [2].

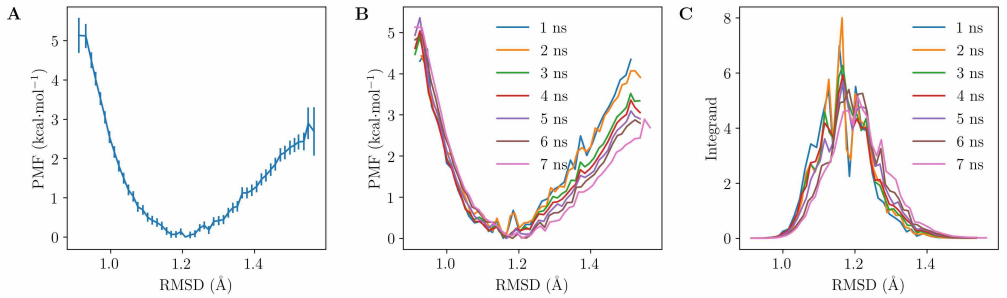

Figure S12: tBRI1 conformational restraint contributions for unbound apo BRI1-BAK1. **A** The restraint PMF. **B** Convergence of the restraint PMF with simulation time. **C** Convergence of the integrand within the associated ensemble average estimation with time. This figure was produced using Matplotlib 2.2.2 [2].

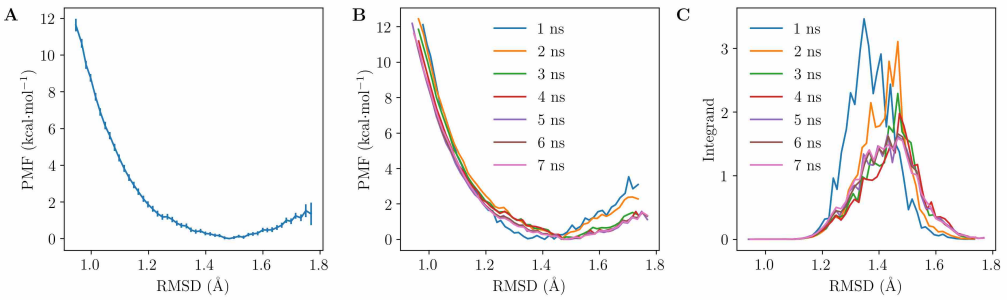

Figure S13: tBRI1 conformational restraint contributions for bound holo BRI1-BAK1. **A** The restraint PMF. **B** Convergence of the restraint PMF with simulation time. **C** Convergence of the integrand within the associated ensemble average estimation with time. This figure was produced using Matplotlib 2.2.2 [2].

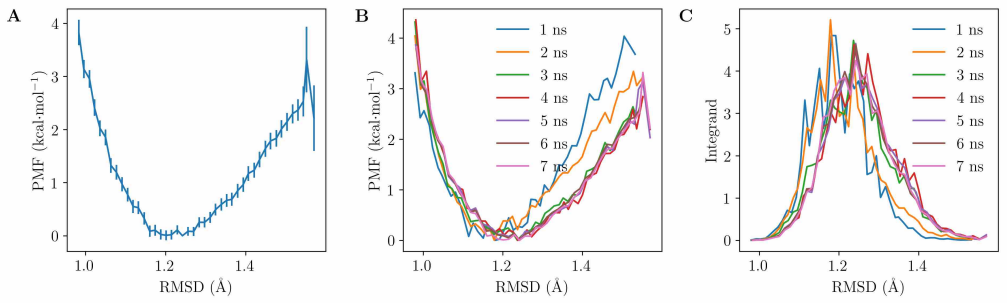

Figure S14: BAK1 conformational restraint contributions for bound holo BRI1-BAK1. **A** The restraint PMF. **B** Convergence of the restraint PMF with simulation time. **C** Convergence of the integrand within the associated ensemble average estimation with time. This figure was produced using Matplotlib 2.2.2 [2].

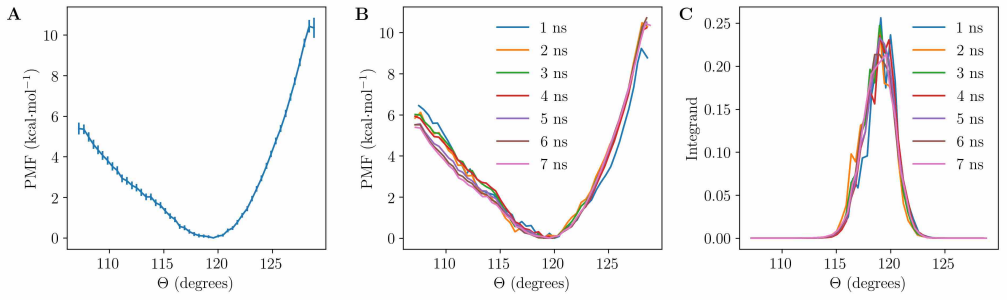

Figure S15: Θ restraint contributions for bound holo BRI1-BAK1. **A** The restraint PMF. **B** Convergence of the restraint PMF with simulation time. **C** Convergence of the integrand within the associated ensemble average estimation with time. This figure was produced using Matplotlib 2.2.2 [2].

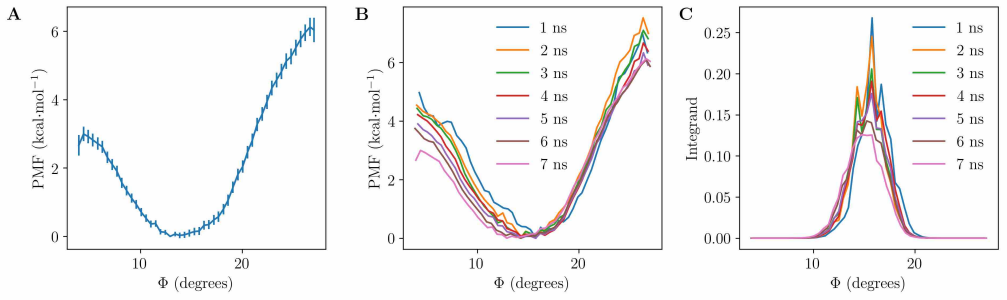

Figure S16: Φ restraint contributions for bound holo BRI1-BAK1. **A** The restraint PMF. **B** Convergence of the restraint PMF with simulation time. **C** Convergence of the integrand within the associated ensemble average estimation with time. This figure was produced using Matplotlib 2.2.2 [2].

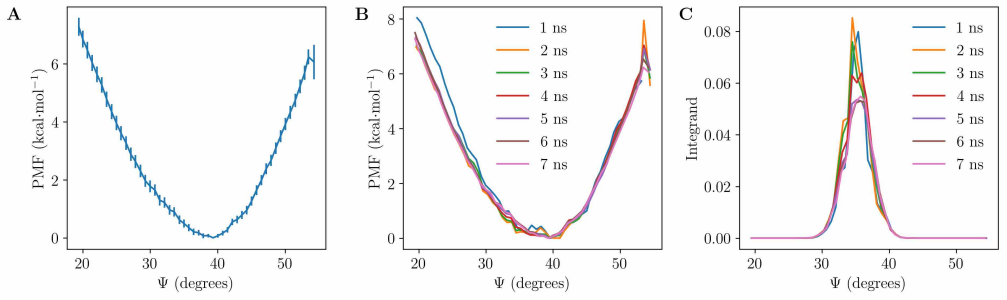

Figure S17: Ψ restraint contributions for bound holo BRI1-BAK1. **A** The restraint PMF. **B** Convergence of the restraint PMF with simulation time. **C** Convergence of the integrand within the associated ensemble average estimation with time. This figure was produced using Matplotlib 2.2.2 [2].

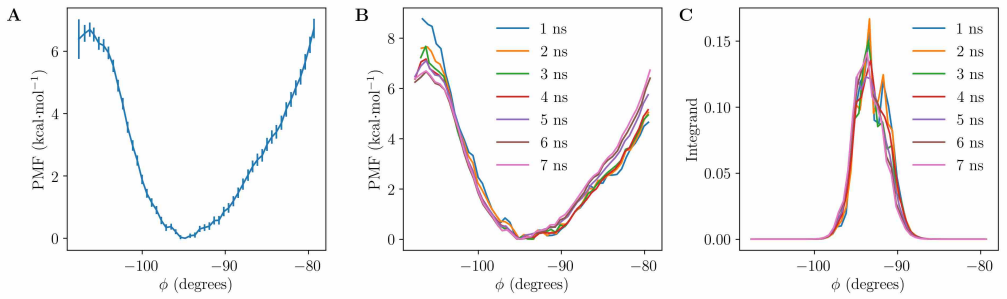

Figure S18: ϕ restraint contributions for bound holo BRI1-BAK1. **A** The restraint PMF. **B** Convergence of the restraint PMF with simulation time. **C** Convergence of the integrand within the associated ensemble average estimation with time. This figure was produced using Matplotlib 2.2.2 [2].

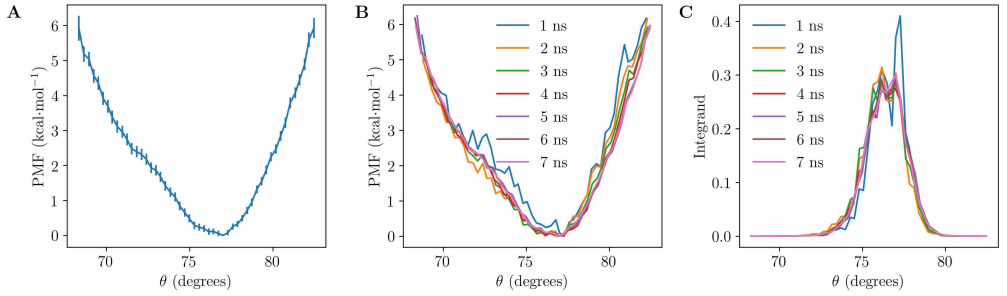

Figure S19: θ restraint contributions for bound holo BRI1-BAK1. **A** The restraint PMF. **B** Convergence of the restraint PMF with simulation time. **C** Convergence of the integrand within the associated ensemble average estimation with time. This figure was produced using Matplotlib 2.2.2 [2].

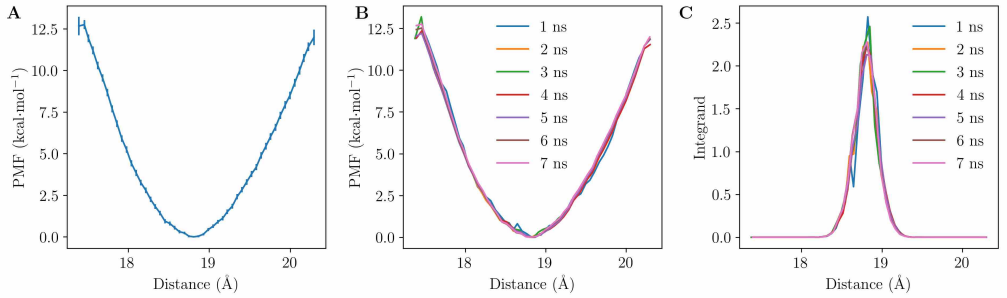

Figure S20: BL restraint contributions for bound holo BRI1-BAK1. **A** The restraint PMF. **B** Convergence of the restraint PMF with simulation time. **C** Convergence of the integrand within the associated ensemble average estimation with time. This figure was produced using Matplotlib 2.2.2 [2].

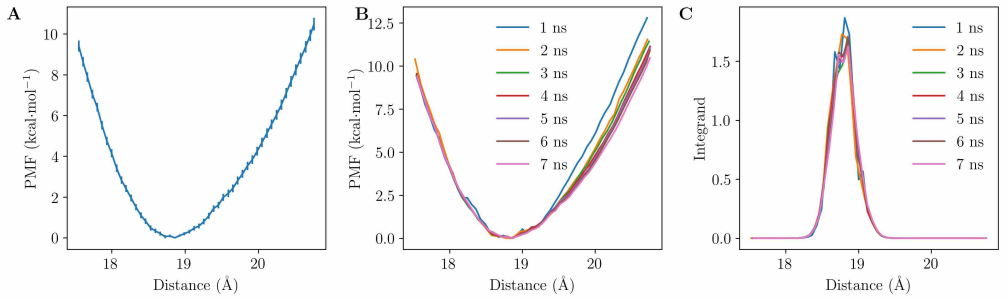

Figure S21: BL restraint contributions for unbound holo BRI1-BAK1. **A** The restraint PMF. **B** Convergence of the restraint PMF with simulation time. **C** Convergence of the integrand within the associated ensemble average estimation with time. This figure was produced using Matplotlib 2.2.2 [2].

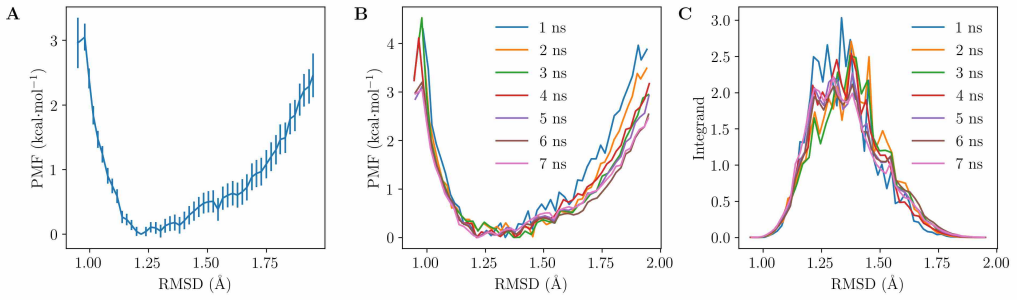

Figure S22: BAK1 conformational restraint contributions for unbound holo BRI1-BAK1. **A** The restraint PMF. **B** Convergence of the restraint PMF with simulation time. **C** Convergence of the integrand within the associated ensemble average estimation with time. This figure was produced using Matplotlib 2.2.2 [2].

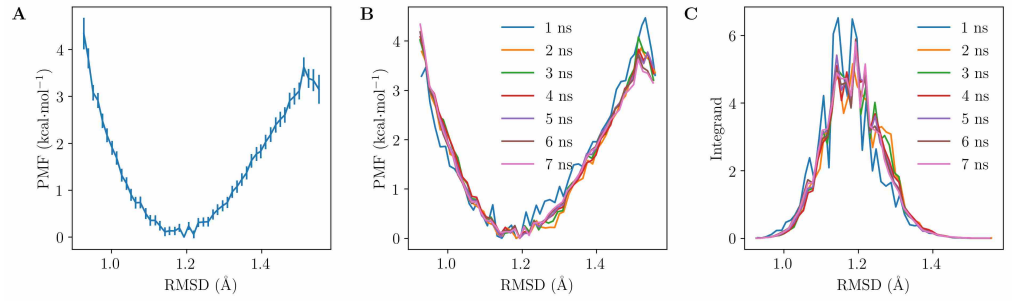

Figure S23: tBRI1 conformational restraint contributions for unbound holo BRI1-BAK1. **A** The restraint PMF. **B** Convergence of the restraint PMF with simulation time. **C** Convergence of the integrand within the associated ensemble average estimation with time. This figure was produced using Matplotlib 2.2.2 [2].

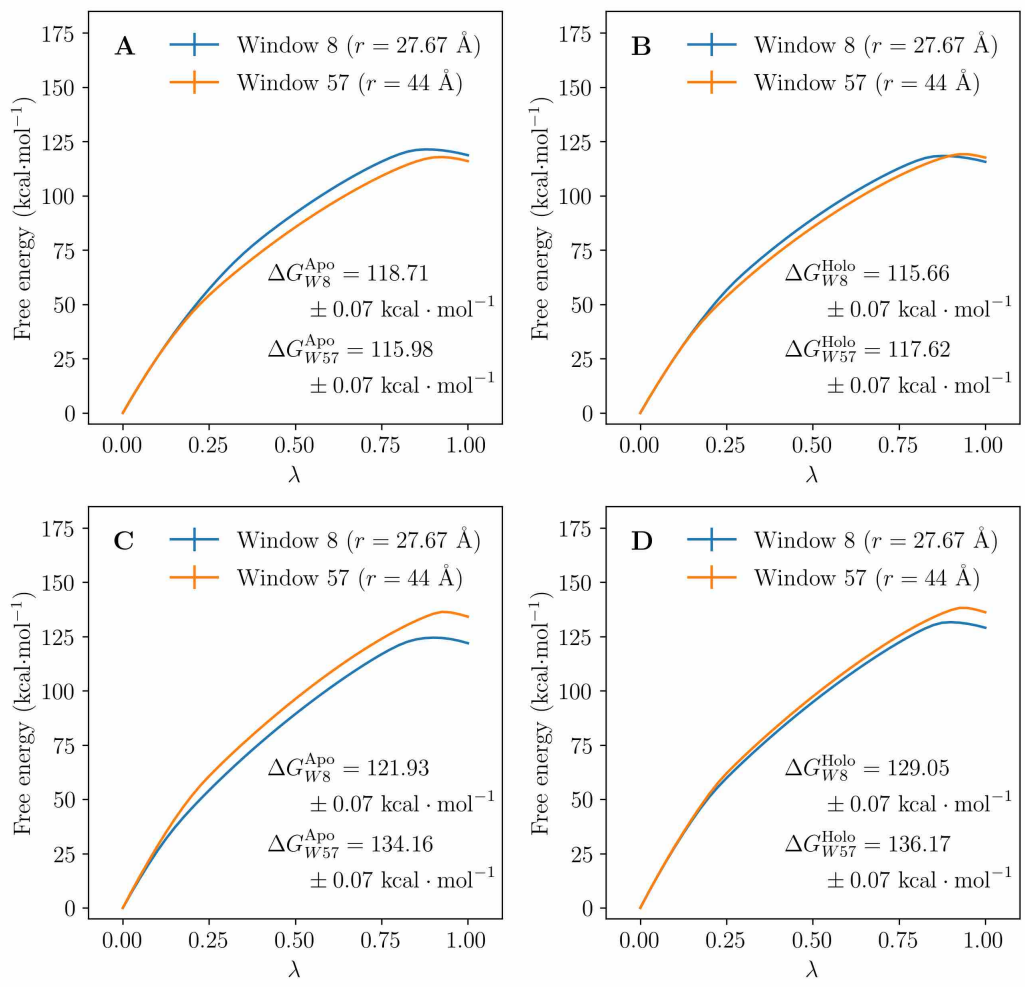

Figure S24: Results from alchemical free energy calculations describing protonation of BAK1 H61 and BRI1 E749, each performed with BRI1 and BAK1 close (window 8, $r = 27.67$ Å) and distant (window 57, $r = 44.00$ Å). On the x-axis is the alchemical parameter λ while on the y-axis is the MBAR-derived relative free energy of each state. **A** Protonation of apo BAK1 H61. **B** Protonation of holo BAK1 H61. **C** Protonation of apo BRI1 E749. **D** Protonation of holo BRI1 E749. This figure was produced using Matplotlib 2.2.2 [2].

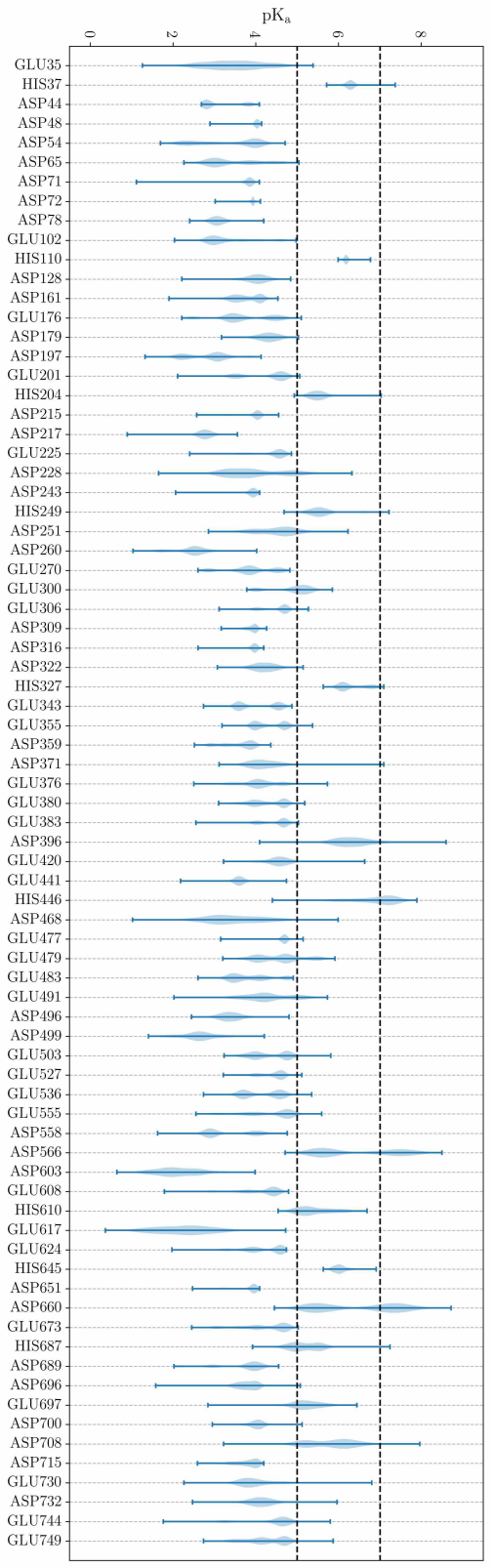

Figure S25: Violin plot of BRI1 sidechain pK$_a$s for residues with sidechain pK$_a$s close to 5, calculated from the simulations of the full, apo BRI1 ECD using PROPKA 3.1 [6, 7]. Frames were taken from apo BRI1 simulations at a rate of 10 ns^{-1}. Bars represent the interval from the lowest to the highest calculated pK$_a$ over all frames. This figure was produced using Matplotlib 2.2.2 [2].